

(AGN)²

11. Heavy Elements and High-Energy Effects

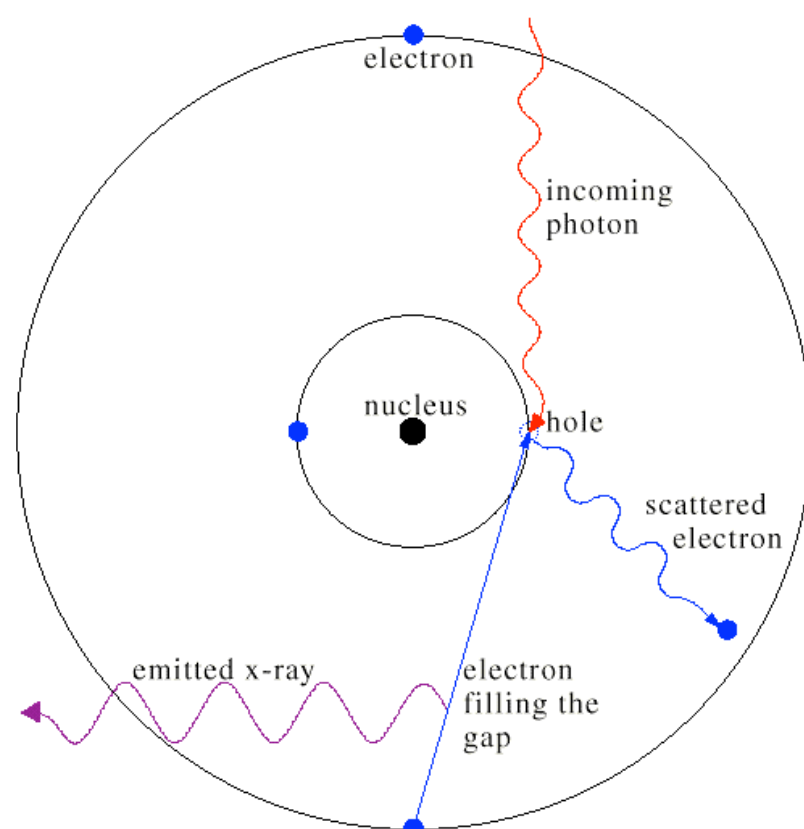
Week 13
May 27 (Monday), 2024

updated on 05/27 13:17

선광일 (Kwangil Seon)
KASI / UST

11.1 Introduction

- High energy effects
 - High-energy photons are able to remove electrons from inner-electron shells of the heavy-element atoms and ions.
 - Cosmic rays both ionize and heat diffuse gas.
 - High energy effects leads to a variety of physical processes that are not ordinarily important in nebulae excited by stellar radiation, but can be important in objects ionized by strong non-stellar continua, such as some supernova remnants and active galactic nuclei.
- X-ray spectroscopy
 - **Recombination** and **collisionally excited** emission lines are present
 - In addition, there are also **fluorescence** lines that are produced when X-rays remove electrons from inner shells of the heavy elements



11.2 Physical Processes Involving Bound Electrons

- Relativistic effects
 - As Z increases, the attractive electron-nucleus Coulomb potential increases, and the velocity of an electron increases to relativistic level.
 - The electrostatic interaction between electrons weakens, and the total angular momentum of individual electrons needs to be considered.
 - For high- Z atoms, this leads to **jj coupling** where j is sum of the individual total electron angular and spin momenta:

$$j_i = l_i + s_i, \quad J = \sum_i j_i$$

where J is the total angular momentum of all electrons in the atom with multiplicity or degeneracy $2J+1$.

- The energy-level splittings and processes dependent on relativistic and inter-electron interactions leads to significant differences in spectral formation for ions within the same isoelectronic sequence.
- LS coupling is applicable when relativistic effects are not important.
- In X-ray nomenclature,
 - $K(1s^2)$, $L(2s^2, 2p^6)$, $M(3s^2, 3p^6, 3d^{10})$, and $N(3s^2, 3p^6, \dots)$
 - The L shell have three energetically distinct levels, $L_1(2s_{1/2})$, $L_2(2p_{1/2})$, $L_3(2p_{3/2})$.

11.2.1 Inner-shell photoionization

- X-ray photons can remove inner-shell electrons.
- Normal order of filling subshells
 - The $4s$ N shell electrons have relatively large probability density near the nuclear, which penetrate the M shell, and are more tightly bound to the atom than $3d$.
 - As a result, the ground electronic configuration of Fe^0 (atomic number = 26) is $1s^2 2s^2 2p^6 3s^2 3p^6 3d^6 4s^2 5D_4$.

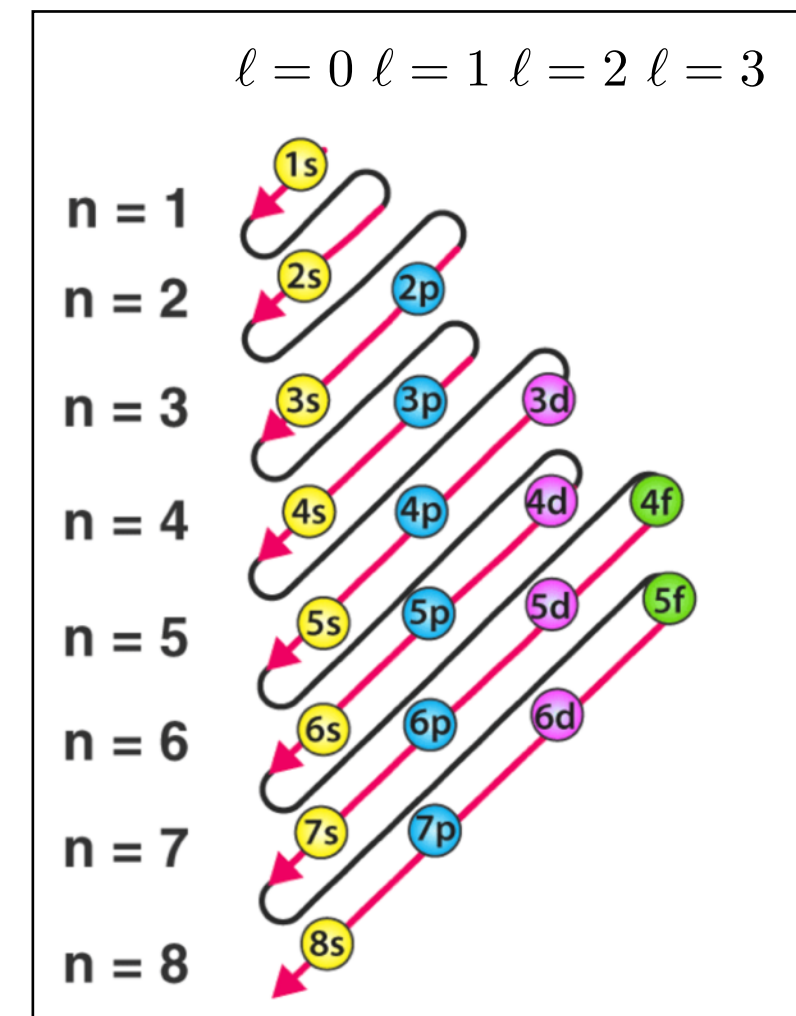
- Transitions

- $K\alpha$: transition from the L to K shell ($1s \leftrightarrow 2p$)

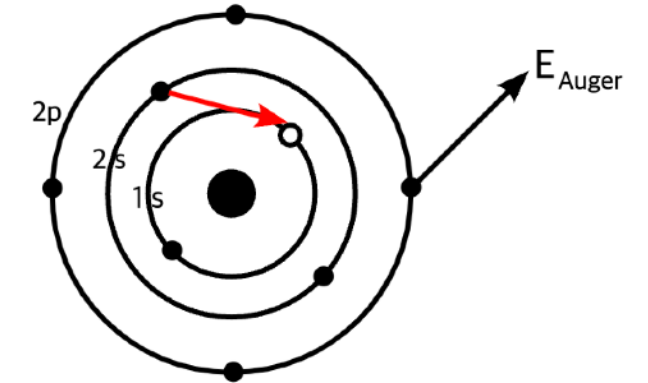
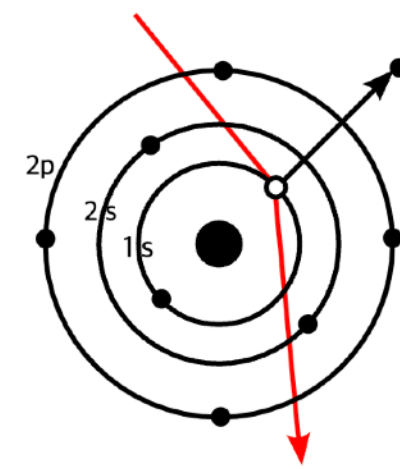
$K\beta$: transition from the M to K shell

Each of these transitions consists of several lines, each between distinct subshells within the main electron shell - for example, $K\alpha$ has components $L_2 - K$ and $L_3 - K$.

$$1s^2 2s^2 2p^6 3s^2 3p^6 4s^2 3d^{10} 4p^6 \dots$$



- Total photoionization cross section
 - is the sum of the photoionization cross sections for each shell that is energetically accessible.
- Fluorescence and Auger effect
 - At energies that are substantially higher than the valence threshold, a photon is more likely to remove an inner-shell electron rather than a valence one.
 - This leaves an inner-shell vacancy or “hole”, which can then be filled by outer electrons “jumping” down, conserving energy by emitting photons (termed **fluorescence**) and by ejecting outer electrons (the **Auger effect**).



- Excitation-autoionization
 - Excitation to levels above the valence shell is also possible.
 - For Be^0 with ground configuration $1s^2 2s^2$, excitation of a $1s$ electron by absorption of a $\text{Be I K}\alpha$ line produces $1s 2s^2 2p$.
 - In this case, the excitation energy exceeds the energy needed to ionize Be^0 and then the autoionization process usually occurs.

- Fluorescent yield
 - the fraction of inner shell holes that are filled by emission of a photon.
 - **Heavy elements like Fe produce rich fluorescent spectra.**

However, fluorescent emission is unlikely for light elements like C or O. Rather, the Auger effect, in which an outer electron moves down to fill the inner vacancy while a second outer electron is ejected, occurs.

Emission of a fluorescent spectrum and Auger electrons occurs to some extent for all elements.

- Efficiency of Auger electron ejection depends on the ability of bound electrons to be rearranged without emission of a photon, which in turn depends on coupling between bound electrons.
- The fluorescent emission efficiency depends on the transition probabilities for the radiative decays to fill the vacancy.
- Transition probability: $A_Z = Z^4 A_1$ along an isoelectronic sequence (Z = nuclear charge).
The rate for a $1s \leftarrow 2p$ decay increases dramatically as atomic number increases and the fluorescent yield increases, too.

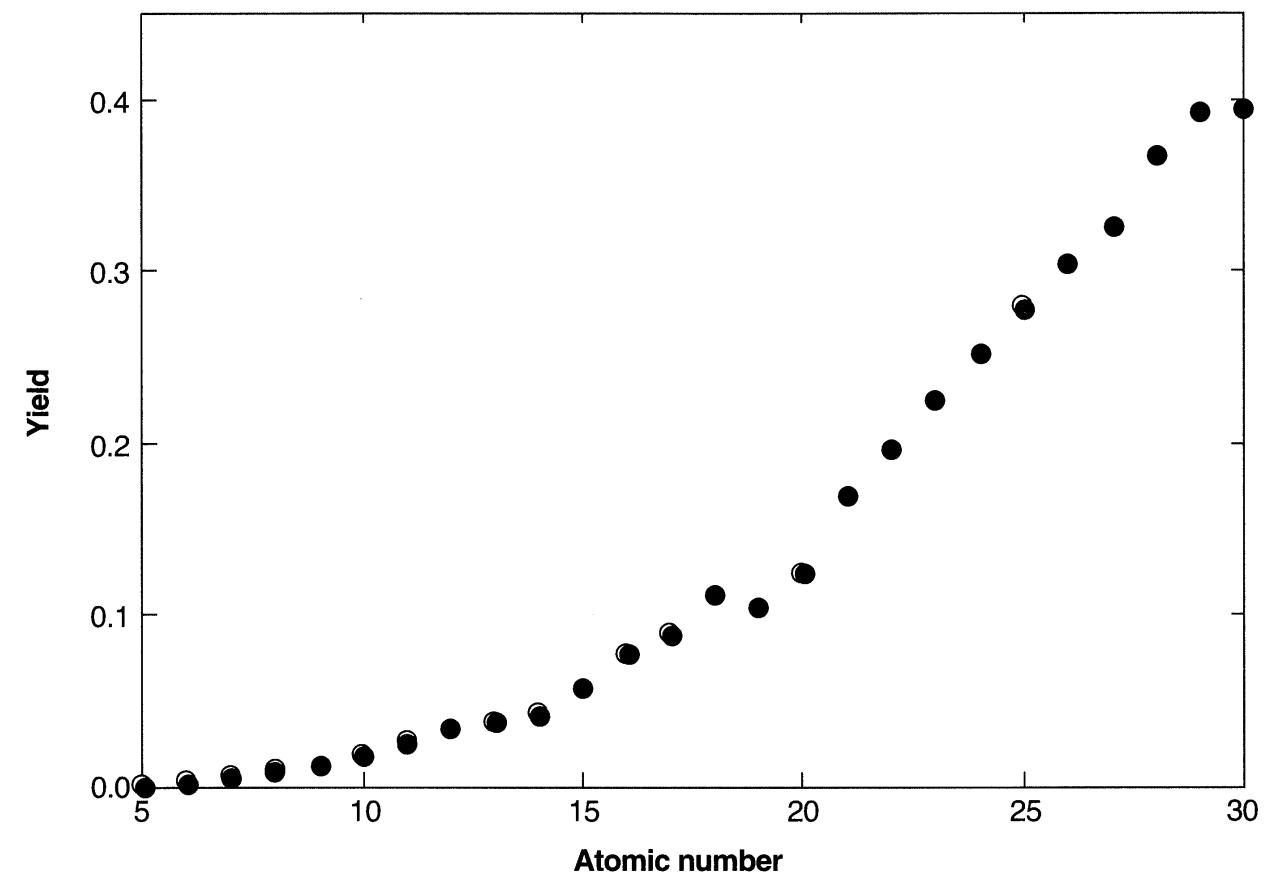


[Figure 11.3]

The probability of filling a vacancy in the K-shell by emitting a $K\alpha$ transition for atoms of the lightest 30 elements.

-
- Energy of Auger electron
 - The kinetic energy of the ejected Auger electron is the difference in energy between the inner-shell hole and the energy of the valence shell, which is less the ionization energy of the valence shell.
 - The K α energy difference is generally very large, $\sim 75\%$ of the ionization energy.
 - Therefore, the Auger electron is ejected with a very high energy: ~ 500 eV for O 0 and many keV for Fe 0 .
 - Fe has the largest fluorescence yield (among astrophysically abundant elements).
 - The emissivity of a fluorescent line is

$$4\pi j_l = n_{\text{ion}} h\nu_l Y_l \int_{\nu_1}^{\infty} \frac{4\pi J_\nu}{h\nu} \sigma_\nu d\nu \quad [\text{erg cm}^{-3} \text{s}^{-1}]$$

Y_l = yield

$h\nu_l$ = line energy

n_{ion} = ion density

ν_1 = ionization threshold for the inner shell

[Table 11.1] K α energies and yields for some heavy elements

Atom	E(K α) (keV)	$\lambda(K\alpha)$ (Å)	Yield
Si 0	1.74	7.10	0.042
S 0	2.31	5.35	0.078
Ar 0	2.96	4.18	0.112
Ca 0	3.69	3.35	0.124
Fe 0	6.40	1.93	0.304

The fluorescence and Auger ejection are fast enough to fill vacancies soon after they are created.

- Heavy elements like Fe produce rich spectra of Auger electrons and fluorescence photons.

K-shell vacancies typically result in the ejection of 6 electrons, with the number of electrons decreasing with higher shells, and higher stages of ionization.

The removal of a $1s$ electron of Fe^0 produces ions as high as Fe^{+9} and a fluorescent spectrum that includes dozens of lines throughout the FUV to X-ray spectrum.

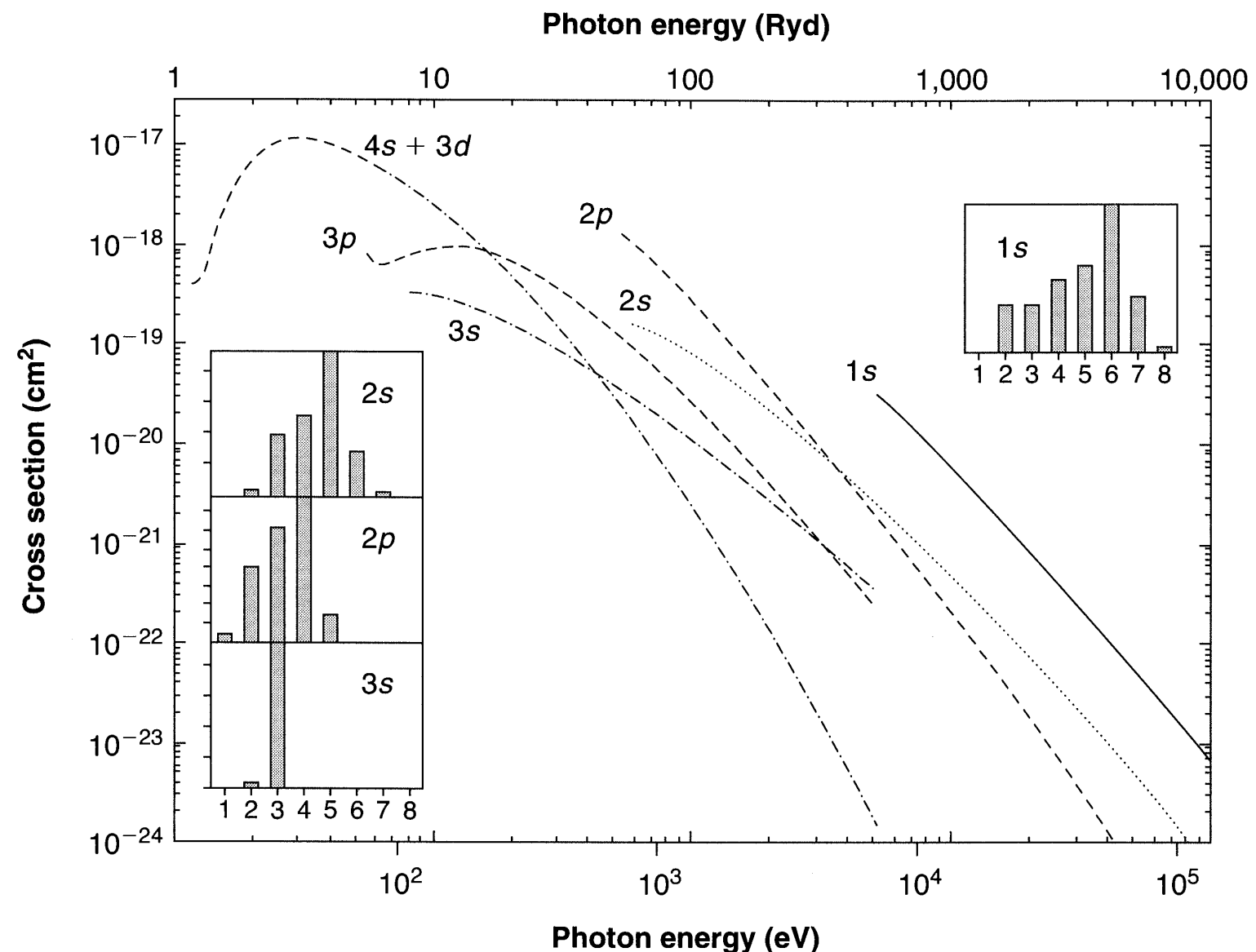


[Figure 11.2]

The total photoionization cross section of Fe^+ . Each subshell is indicated at the threshold of the curve. The insert bar graphs show the relative numbers of Auger electrons produced from each shell.

- Energies of the $K\alpha$ transitions for various stages of ionization of Fe
 - [reference] the non-relativistic energy of the hydrogenic $Ly\alpha$ transition $\sim 0.75 \times 13.56 \times Z^2$ eV = 6.87 keV ($Z = 26$)
 - $K\alpha$ energy of Fe XXVI = 6.97 keV (slightly different from the non-relativistic formula)
 - $K\alpha (1s^2 \leftarrow 1s 2p)$ energy of Fe XXV = 6.72 keV, lower because of the screening of part of the nuclear charge by the other $1s$ electron. (The screening is caused by the charge distribution that is inside the charge distribution of the other electron.)
 - $K\alpha (1s^2 2s \leftarrow 1s 2s 2p)$ of Fe XXIV has an additional (but smaller) amount of screening from the $2s$ electron. (because the wavefunction of $2s$ inside the $1s$ charge distribution is much smaller.)
 - The next $2s$ electron and each additional $2p$ electron through $2p^5$ adds further additional screening, but the higher $3s$, $3p$, and $3d$ wavefunctions have charge densities inside the $1s$ orbit too small to be effective.
 - Therefore, this shift in the energy of $K\alpha$ makes this transition an ionization indicator (although a coarse one when the energy resolution is modest.)
 - The older X-ray astronomy literature refers to the first ~ 17 ionization stages of Fe as “cold” iron, and higher ionization states, as “hot” iron.

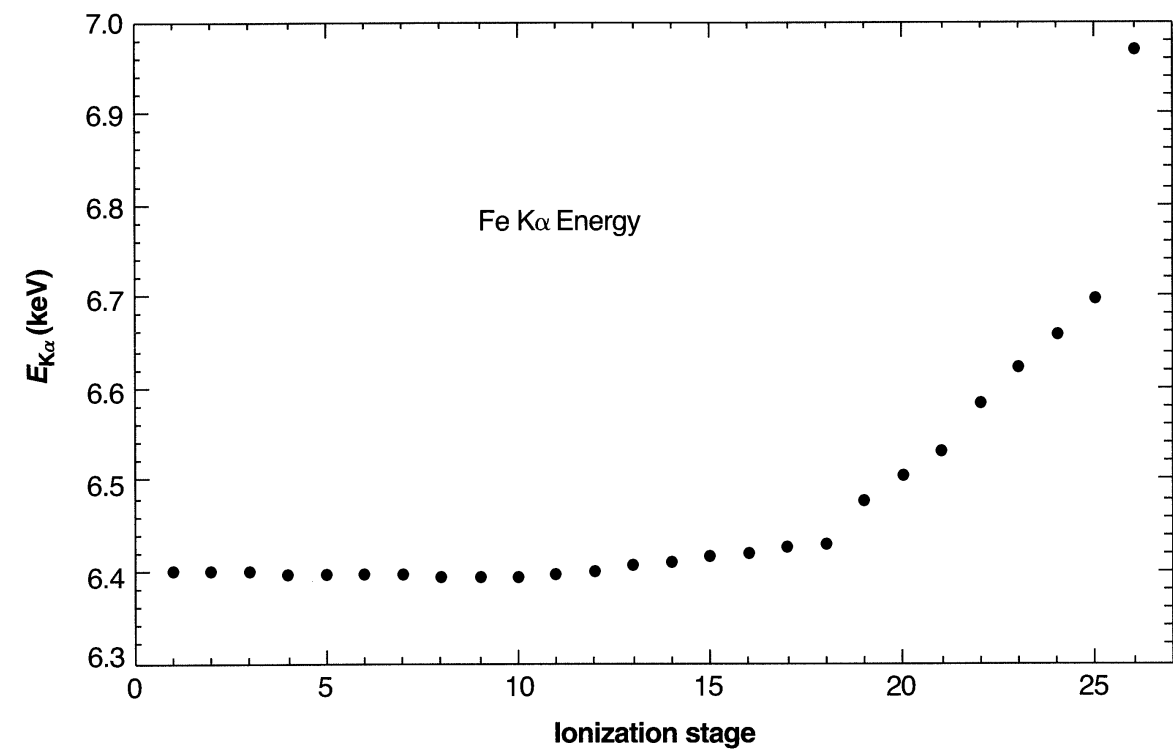
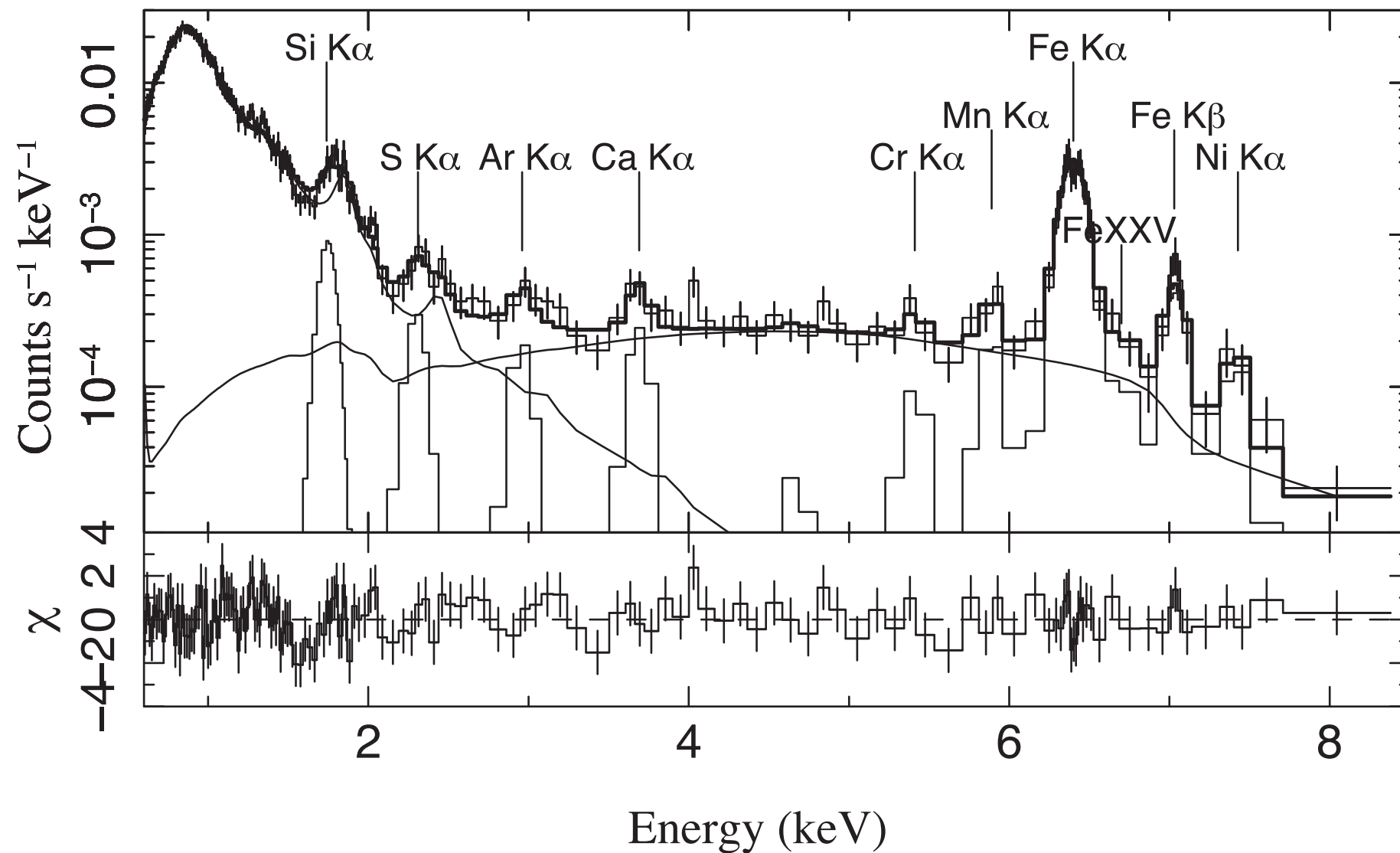


[Figure 11.4]
K α energies for ions of Fe.



X-ray fluorescent lines from the Compton-thick AGN in M51 (Xu et al. 2016, MNRAS, 455, L26)

The model of Vapec + MYTorus + Gaussians fitted to the Chandra spectrum of the nucleus of M51. The residuals around the added K α lines are reduced significantly. The model line feature around 4.6 keV is the instrumental Si escape peak, which follows the Fe 6.4 keV line and is about 1% of the Fe line intensity.

- [Figure 11.5] shows the total photoelectric cross sections for an ionized gas with a cosmic abundances.
 - The inner shell cross section shown in Figure 11.2 do not have a strong dependence on the ionization stage (the $K\alpha$ energy does not change for cold Fe.)
- **These energies and cross sections also do not change greatly if the atom is in a grain**, since the binding energy within the grain material is small compared with the inner-shell energies.

The opacity for a unit hydrogen density, solar composition, and neutral gas

The hydrogen curve shows the cross section for photoionization of hydrogen.

The curve marked “heavy element photoelectric” includes all opacities that remove electrons from a moderately ionized gas.

Inner-shell processes cause the edges between 100 and 10,000 eV.

The increase at higher energies is caused by Compton-recoil ionization. The electron scattering cross section is at the Thomson value of low-photon energies, and goes over to the Klein-Nishina relativistic limit at high-photon energies. The cross section for pair production is also shown.

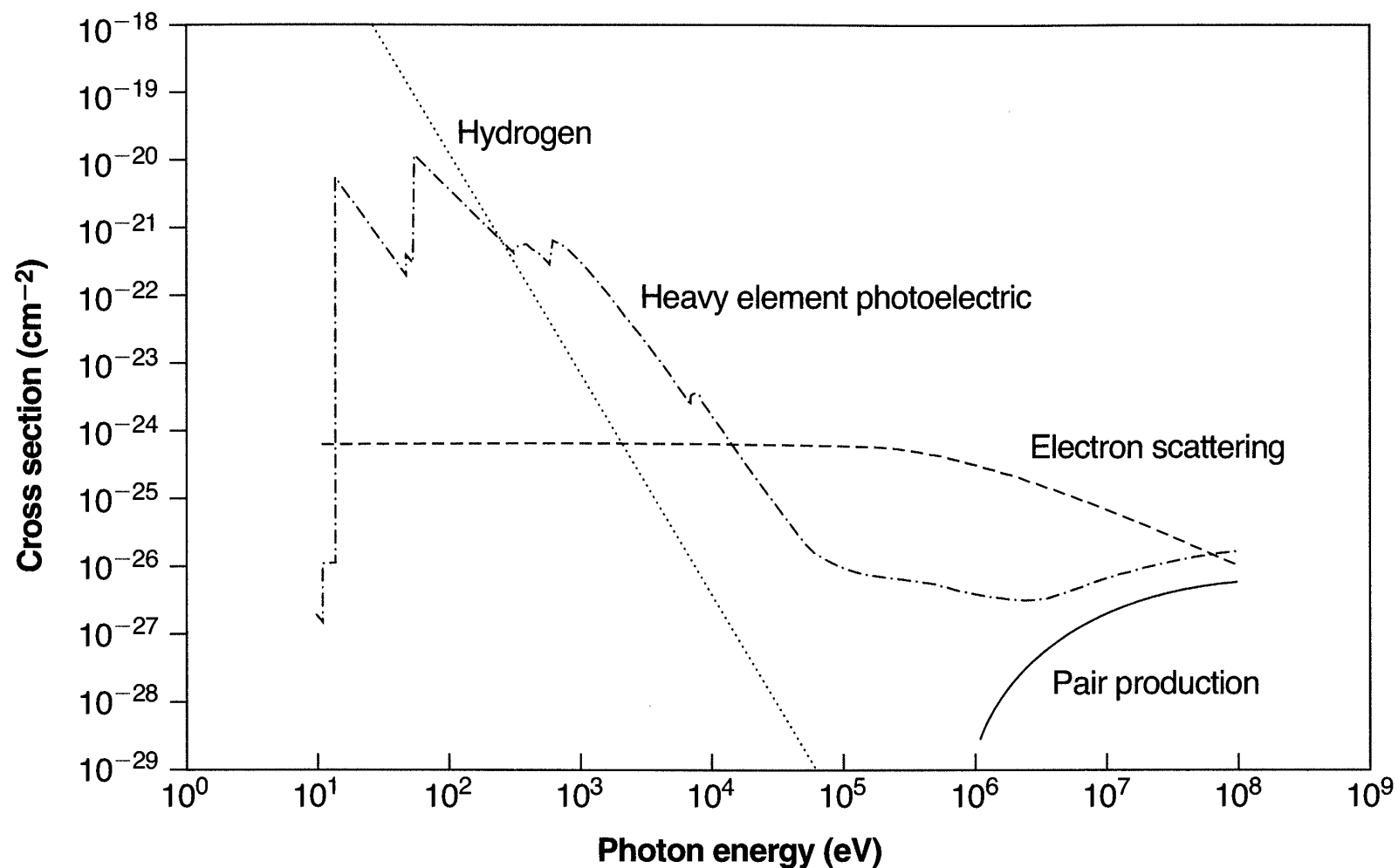


[Figure 11.5]
Comparison of the total opacity due to several of the processes

11.3 Physical Processes at Still Higher Energies - 11.3.1 The Compton Effect

- Photons can interact with matter by Compton energy-exchange, a process in which photons are scattered by an electron.
 - Thomson electron-scattering cross section $\sigma_T = 8\pi r_0^2/3 = 6.65 \times 10^{-25} \text{ cm}^2$.
 - If a single photon is scattered by an electron at rest, the wavelength of the photon is decreased by an amount that depends on the angle by which it is scattered, according to the Compton formula: $\lambda - \lambda_0 = \frac{h}{m_e c} (1 - \cos \theta)$
 - In an astronomical plasma, the electrons have a thermal velocity distribution and the relative energy shift is $\frac{\delta h\nu}{h\nu} = \frac{4kT}{m_e c^2}$.
 - **Inverse Compton scattering:** If $kT > h\nu$, the photon can gain energy.

The net rate of electron heating or cooling is given by:

$$H_{\text{Comp}} = \frac{4\pi n_e}{m_e c^2} \int \sigma_T J_\nu (h\nu - 4kT) d\nu \quad [\text{erg s}^{-1} \text{ cm}^{-3}]$$

Compton energy exchange can be important. All nebulae are irradiated by the 2.7 K “cosmic background”, which acts as a coolant. In Chapter 14, we shall see that inverse Compton scattering may produce the UV continuum of a quasar.

-
- Compton-recoil ionization
 - Compton recoil can result in ionization of an atom or ion if the recoil energy exceeds the binding energy of an electron.

The recoil energy E is given by

$$E = h\nu \left(1 - \frac{1}{1 + h\nu/m_e c^2} \right), \text{ where } h\nu \text{ is the incident photon energy.}$$

- A simple rearrangement shows that photons with energies greater than $h\nu = \sqrt{\chi_0 m_e c^2}$ can ionize an atom or ion with ionization potential χ_0 .

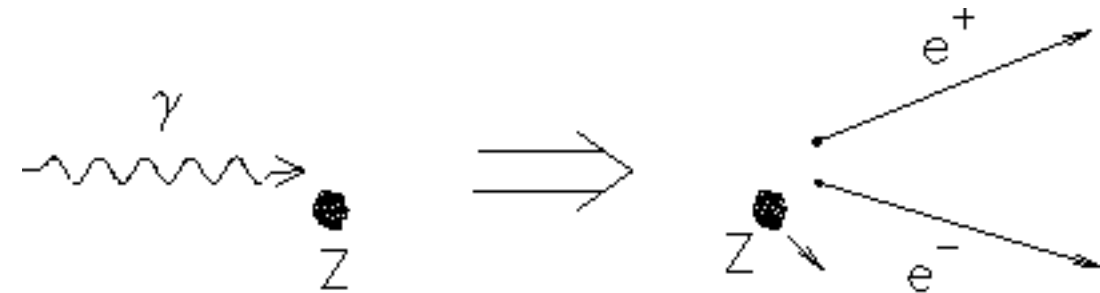
$$\Leftarrow \quad \chi_0 = h\nu \left(1 - \frac{1}{1 + h\nu/m_e c^2} \right) \approx h\nu \frac{h\nu}{m_e c^2}$$

Photons with energies greater than ~ 2.3 keV can ionize hydrogen by Compton recoil.

Compton-recoil ionization is more likely than photoionization for very high-energy photons due to the $\sim (\nu/\nu_0)^{-3}$ fall off in the hydrogen photoionization cross section.

11.3.2 Pair production

- Photons with energies greater than $2m_e c^2$ continuously undergo pair production, forming virtual $e^+ - e^-$ pairs.
 - They cannot become a real pair in a vacuum, while conserving both energy and momentum, because the pair, once formed, must separate with finite kinetic energy.
 - However, if the virtual pair forms in the electric field of a nucleus, it can transfer momentum to the nucleus and become a real pair.
 - The cross section for this process depends on energy and charge but is typically $\sim 10^{-27} \text{ cm}^{-2}$. The resulting pair eventually annihilates, forming an emission line at 0.511 MeV.

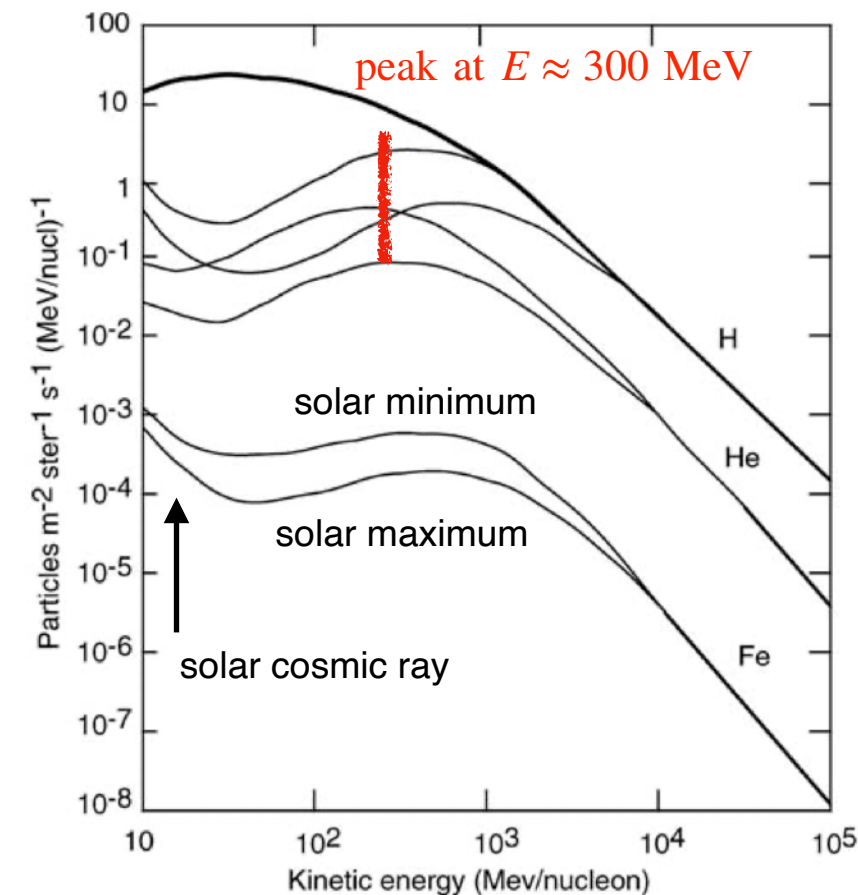


11.3.3 Secondary ionization by suprathermal electrons

- Suprathermal electrons
 - Auger electrons, electron-positron pairs produced in pair production, and photoelectrons produced by high-energy continua, all have initial kinetic energies that can be much larger than kT .
 - **In an ionized gas**, their kinetic energy of the “suprathermal” electrons is converted into heat through frequent elastic collisions with thermal electrons.
- “**knock-on**” or secondary electrons
 - **In a neutral gas**, they may cause collisional ionization or line excitation before interacting with free electrons.
 - A high-energy electron can create a second suprathermal electron if it collisionally ionizes an atom. This occurs many times, creating a shower of suprathermal electrons, often referred to as “knock-on” or secondary electrons, before they eventually reach thermal energies.
 - These electrons can also excite strong allowed lines like H I Ly α .
 - A single high-energy electron can produce a substantial number of ionizations and excitations and can deposit relatively little energy as heat.
- Importance of secondary ionization
 - The ionization fraction $x = n(\text{H}^+)/n(\text{H})$ determines the importance of secondary ionization, since this ratio is proportional to the probability that a fast electron will share its energy with a free electron, compared with its probability of striking an atom or molecule.
 - Most kinetic energy goes into heat when $x > 0.9$.
 - If $x \ll 0.9$, much of an energetic primary electron’s energy goes into secondary ionization ($\sim 40\%$ into H^0 ionizations) and excitation ($\sim 40\%$ into H I excitations, mainly Ly α), and less into heat ($\sim 14\%$).

11.3.4 Cosmic rays

- Cosmic rays are nuclei and electrons with relativistic energies.
 - protons (~90%), helium nuclei (~8%), heavier nuclei (~1%), and other (~1%; electrons, positrons, and antiprotons)
 - They are believed to have been accelerated to energies approaching 10 GeV by supernovae and are trapped by the magnetic field of the Galaxy.
 - Lower-energy cosmic rays cannot be directly observed from the Earth because of the magnetic field of the solar system, but the galactic (cosmic ray) background is inferred indirectly from their observed effects.
 - ▶ Synchrotron emission is one observed product of the presence of cosmic rays, another is low level of ionization even deep within molecular clouds.
 - ▶ Their density distribution can be fitted as a power law, $n_{\text{cr}} \propto E^{-2.4}$.
- Cosmic rays can both heat and ionize gas in neutral or molecular regions that are shielded from ionizing radiation.
 - The unobservable low-energy cosmic rays have the greatest effects upon the neutral and molecular gas due to their large number.
 - The H^0 ionization rate due to the galactic cosmic ray background is $\sim 2 \times 10^{-17} \text{ s}^{-1}$. These ionizations produce an electron with ~ 35 eV of energy, which will then create secondary electrons.



Differential energy spectra of cosmic-ray protons (H), α particles (He), and iron, near solar minimum and maximum (Silberberg et al. 1988)

11.3.5 Total opacity

- Figure 11.5
 - H, He, and grains (when present) are generally the most important opacity sources at energies lower than several times the ionization threshold of He^+ (54 eV).
 - At much higher energies, the inner shell opacities of the heavy elements are important, and Auger ejection affects the level of ionization of the gas.
 - At considerably higher energies, Compton recoil becomes important, both as an opacity source and in ionizing the gas.
 - Each opacity source affects the total heating of a cloud if the cloud is optically thick to that opacity source.

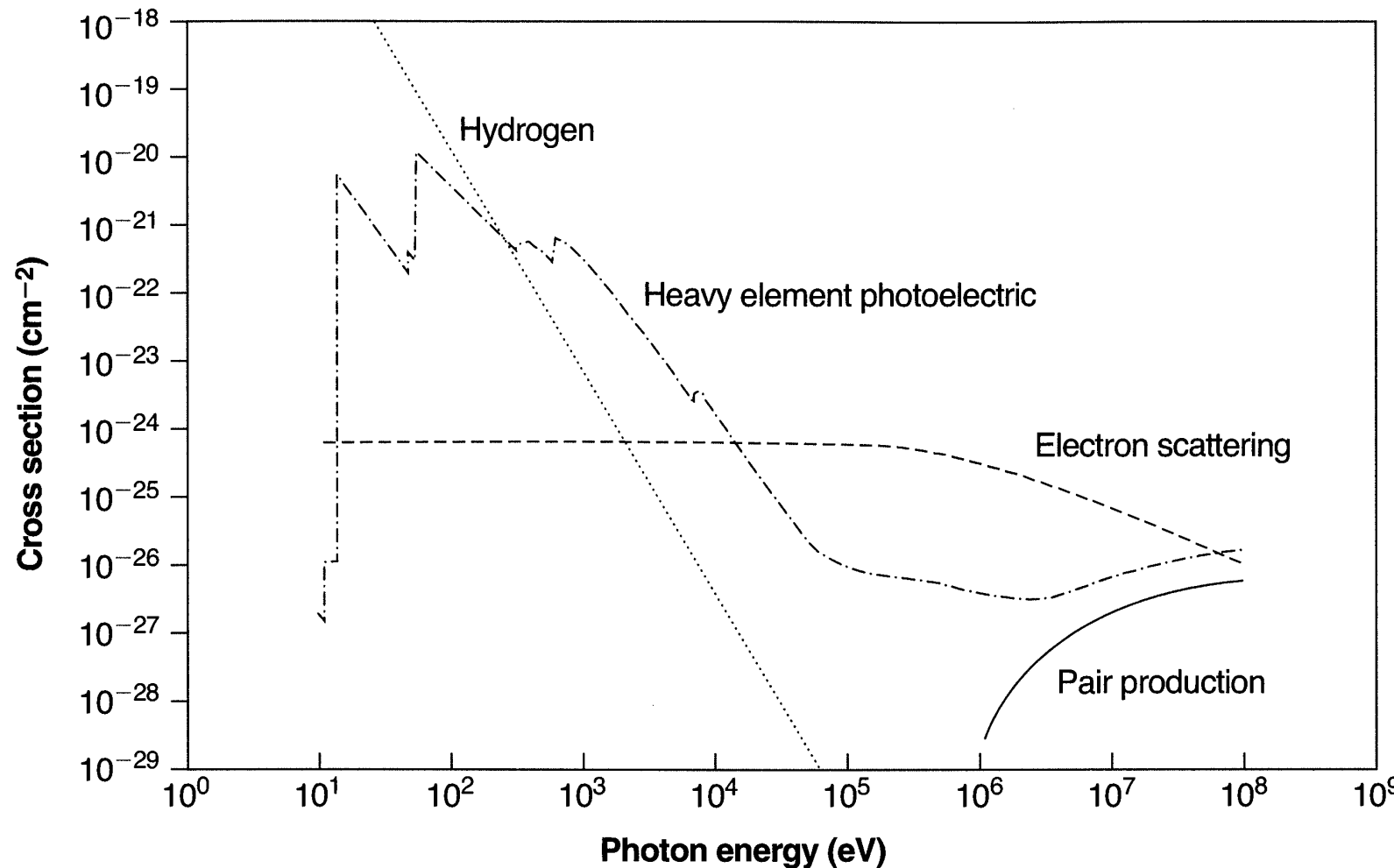
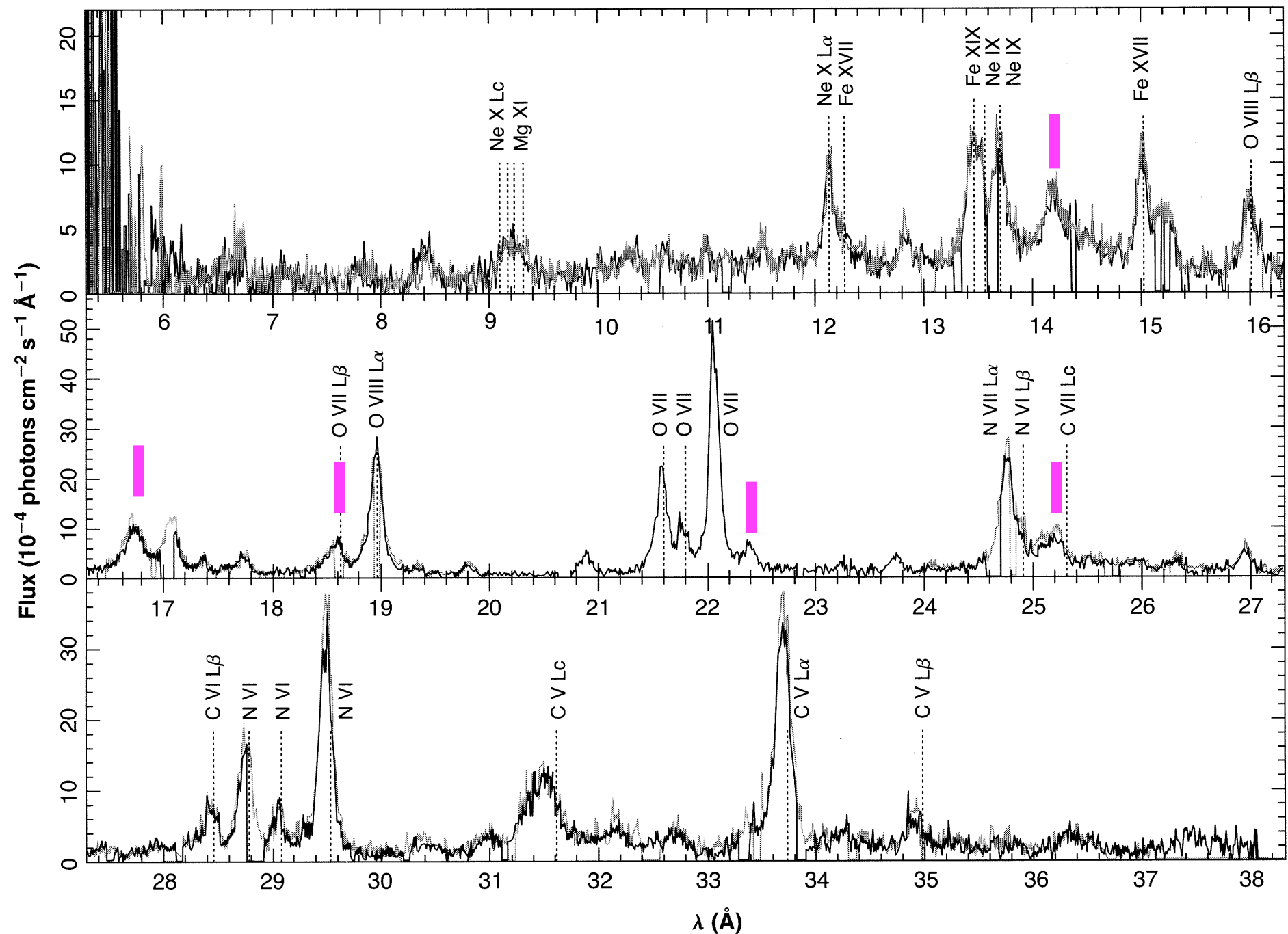


[Figure 11.5]
Comparison of the total opacity due to several of the processes

11.4 Physical Conditions from X-ray Spectroscopy

- [Figure 11.6]
 - The **soft X-ray** spectrum of an active galactic nucleus NGC 1068 (Seyfert galaxy).
The spectrum shows emission lines and recombination continua.
The underlying physics is the same as in H II regions, but some of the details are different.



■ represents the recombination continua.

The widths correspond to $T \approx 40,000$ K.

[Note]
 $1 \text{ keV} = 12.40 \text{ \AA}$

- The X-ray spectrum is divided into “hard” ($h\nu \lesssim 2$ keV) and “soft” ($h\nu \gtrsim 2$ keV) because of practical aspects of detector technology.
 - The lighter astrophysically abundant elements ($Z \leq 14$, lighter than Si) do not have enough internal energy to produce lines in the hard X-ray region.
 - However, Fe ($Z = 26$) does have prominent lines in this region.
- Isoelectronic sequence (ions with the same number of electrons)
 - H-like : all ions with a single electron
 - He-like : those with two electrons
 - Along an isoelectronic sequence, the transition probabilities scale as Z^4 and energies as Z^2 .
 - **The strongest features in Figure 11.6 are the heavy-element equivalents of $1s \leftarrow 2p$ H I Ly α .**

-
- Both H-like and He-like ions produce strong $1s \leftarrow 2p$ emission lines.

[Table 11.2] H-like $1s - 2p$ wavelength and two-photon critical density

Ion	λ (Å)	$h\nu$ (keV)	$A(2\nu)$ (s^{-1})	$n_{crit}(2s)$ (cm^{-3})
C VI	33.74	0.366	3.8×10^5	5.1×10^{14}
N VII	24.78	0.499	9.7×10^5	1.7×10^{15}
O VIII	18.97	0.652	2.2×10^6	5.0×10^{15}
Si XIV	6.19	2.00	6.2×10^7	4.2×10^{17}
Fe XXVI	1.78	6.94	2.5×10^9	5.8×10^{19}

[Table 11.3] He-like $n = 2$ lines and transition probabilities

Ion	$1s^2 \ ^1S_0 - 1s \ 2s \ ^3S_1$		$1s^2 \ ^1S_0 - 1s \ 2p \ ^3P_1^o$		$1s^2 \ ^1S_0 - 1s \ 2p \ ^1P_1^o$	
	λ (Å)	A (s^{-1})	λ (Å)	A (s^{-1})	λ (Å)	A (s^{-1})
C V	41.46	6.9×10^3	40.74	2.6×10^7	40.27	8.9×10^{11}
N VI	29.53	249	29.09	1.4×10^8	28.79	1.8×10^{12}
O VII	22.10	1000	21.81	5.5×10^8	21.60	3.3×10^{12}
Si XIII	6.743	3.4×10^5	6.687	1.5×10^{11}	6.645	3.8×10^{13}
Fe XXV	1.867	3.9×10^9	1.856	5.8×10^{13}	1.848	4.6×10^{14}

- Recombination
 - In a photoionized gas, the lines are almost entirely produced by recombination since the gas temperature is low compared to their excitation energies (which are 3/4 of the ionization energies).
 - ~ 2/3 of recombinations eventually populate $2p$, which produces the Ly α transition.
 - ~ 1/3 of recombinations populate $2s$, which (1) emits a two-photon continuum, or (2) undergoes a $2s - 2p$ collision, which then leads to emission of a Ly α photon.
 - [Table 11.2] shows that the two-photon transition probabilities are substantial because of the large ionic charge.

The critical electron density, at which the probability of a radiative decay is equal to the probability of a $2s - 2p$ collision, is correspondingly high. As a result, most observed emission-line environments are in the low-density limit.
- Case A, Case B, Case C
 - Case A assumes that (1) the gas is optically thin in the Lyman lines and (2) the continuum striking the clouds contains no radiation within the higher- n Lyman lines. (no continuum-pumped Lyman series)
 - Case B assumes that it is optically thick in all higher Lyman lines. Every photon emitted in a higher Lyman line is eventually degraded into (1) a Balmer line plus a Ly α or (2) two-photon continuum.
 - Case C assumes the case including the continuum which can cause fluorescence through these Lyman lines (Ferland, 1999, PASP, 111, 1524).
 - Figure 11.6 shows higher Lyman recombination lines. Therefore, Case C appears to be present in the gas emitting the spectrum.

- He-like isoelectronic series offers direct density diagnostics.
 - Table 11.3 shows the lines arising from the $n = 2$ levels in addition to the two-photon continuum ($1s^1S \leftarrow 2s^1S$).
 - They have a wide range of transition probabilities making their relative intensities sensitive to density.
 - However, the interpretation is complicated somewhat by the Case B-C transition.
 - These lines have proven valuable density probes for densities of $10^8 - 10^{12} \text{ cm}^{-3}$.

[Table 11.3] He-like $n = 2$ lines and transition probabilities

Ion	$1s^2 1S_0 - 1s 2s 3S_1$		$1s^2 1S_0 - 1s 2p 3P_1^o$		$1s^2 1S_0 - 1s 2p 1P_1^o$	
	$\lambda (\text{\AA})$	$A (\text{s}^{-1})$	$\lambda (\text{\AA})$	$A (\text{s}^{-1})$	$\lambda (\text{\AA})$	$A (\text{s}^{-1})$
C V	41.46	6.9×10^3	40.74	2.6×10^7	40.27	8.9×10^{11}
N VI	29.53	249	29.09	1.4×10^8	28.79	1.8×10^{12}
O VII	22.10	1000	21.81	5.5×10^8	21.60	3.3×10^{12}
Si XIII	6.743	3.4×10^5	6.687	1.5×10^{11}	6.645	3.8×10^{13}
Fe XXV	1.867	3.9×10^9	1.856	5.8×10^{13}	1.848	4.6×10^{14}

-
- Radiative recombination continua
 - O VIII $\lambda 14.2 \text{ \AA}$, O VII $\lambda 16.8 \text{ \AA}$, N VII $\lambda 18.6 \text{ \AA}$, N VI $\lambda 22.5 \text{ \AA}$, and C IV $\lambda 25.3 \text{ \AA}$ (denoted by the **I** symbol)
 - **The recombination continuum appears almost as a broad line with a width $\delta\lambda/\lambda \approx kT/\chi$.**

Note that the recombination rate coefficient is given in Appendix 2:

$$n_e n(X^{+i+1}) u \sigma(u) f(u) du \quad \left(\frac{1}{2} m_e u^2 + h\nu_t = h\nu, \nu_t = \text{threshold frequency} \right)$$

where $\sigma(u) = \frac{\omega_i}{\omega_{i+1}} \frac{h^2 \nu^2}{m_e^2 c^2 u^2} \sigma_\nu^{\text{pi}}$ and $f(u)$ is the Maxwell distribution function.

Recombination preferentially emits from slightly lower energies ($h\nu > h\nu_t$). The width of the continuum produced by a recombination to a level with ionization potential $\chi = h\nu_t$ would be $\delta\lambda/\lambda \approx \delta\nu/\nu_t \approx kT/\chi$ because $\langle 1/2m_e u^2 \rangle \approx kT$.

- For instance, in the case of the hydrogen Balmer continuum ($n = 2 \rightarrow n = \infty$), the ionization potential is $\sim 3.4 \text{ eV}$ ($\leftarrow 12.6/4$), so the recombinations produce a broad feature with $\delta\lambda/\lambda \approx 1/3$.
- However, in the case of heavier elements (Figure 11.6), recombinations are to the ground state, kT/χ is small (χ is large), and **the emission continuum appears almost as a line**.

The width of recombination continuum is a temperature indicator.

The recombination continua shown in the figure correspond to $T \approx 40,000 \text{ K}$.

- Hot gas : X-ray spectroscopy
 - The gas producing the spectrum of Figure 11.6 is hot and very highly ionized.
 - In such high temperature, second-row elements (Li, Be, B, C, N, O, F, Ne) have only 0, 1, or 2 bound electrons.
 - **Hot gas is a strong source of X-rays while producing very little in the optical.**

Optical H and He recombination lines will be produced but their emissivity decreases with increasing temperature and so is small for very hot gas.

The strongest feature in the hard X-ray spectrum is the Fe K α line, an indicator of the level of ionization of Fe as well as the column density.
- Moderate temperature gas
 - is a strong sources of optical and UV emission
 - can produce fluorescent lines if column densities are as large as 10^{24} cm^{-2} or greater.

11.5 Collisional Excitation of H⁰

- Partially ionized regions in AGNs
 - X-rays can easily penetrate through the H⁺ zone of a nebula and enter the neutral gas behind the hydrogen ionization front.
 - They produce a large partially ionized region which contains H⁰, H⁺, and e⁻.
 - Hence, collisional excitation of neutral atoms can occur, and is observed particularly in [O I] λλ6300, 6364, and [N I] λ5199.
 - In addition, **collisional excitation of H⁰ by thermal electrons produces strong Lyα emission, and makes a significant contribution to Hα.**
 - This process occurs in AGNs.
- Collisional excitation of Lyα
 - **Direct collisional excitation** at low densities
 - ▶ H⁰(1s ²S) + e → H⁰(2p ²P^o) + e with a threshold 10.2 eV (~ 1.2 × 10⁵ K).
 - ▶ The emission coefficient is

$$4\pi j_{\text{Ly}\alpha} = n_e n(\text{H}^0) q_{1^2S, 2^2P^o} h\nu_{\text{Ly}\alpha} \quad \text{where} \quad q_{12} = \frac{8.629 \times 10^{-6}}{T^{1/2}} \frac{\gamma(1,2)}{\omega_1} e^{-\chi/kT}$$

Table 3.16

Effective collision strengths for H I

T(K)	1 ² S, 2 ² S	1 ² S, 2 ² P ^o	1 ² S, 3 ² S	1 ² S, 3 ² P ^o	1 ² S, 3 ² D
10,000	0.29	0.51	0.066	0.12	0.063
15,000	0.32	0.60	0.071	0.13	0.068
20,000	0.35	0.69	0.077	0.14	0.073

- **Indirect excitation** of Ly α at high densities (cascading following collisional excitation to $n = 3$)

- ▶ The collisional strengths decrease rapidly with increasing principal quantum number n (Table 11.3), and the threshold energy increases with n , making the contribution to Ly α emission from collisional excitation to higher levels, followed by cascading down to 2^2P^o quite small.

- ▶ Every excitation to 3^2S or 3^2D is followed by emission of H α and then Ly α .

However, every excitation to 3^2P^o leads to emission of H α and population of 2^2S , under Case B conditions, which does not emit Ly α .

- ▶ Thus, the collisional-excitation contribution to the Ly α emission coefficient may be written

$$4\pi j_{\text{Ly}\alpha} = n_e n(\text{H}^0) (q_{1^2S, 2^2P} + q_{1^2S, 3^2S} + q_{1^2S, 3^2D} + \dots) h\nu_{\text{Ly}\alpha}$$

- ▶ Table 11.4 show the Ly α emission coefficients for (1) the direct excitation case at low density and (2) the direct + indirect excitation case at high density, together with those due to recombination.
- ▶ Note that including the still smaller contributions of excitation to the levels $n > 4$ would result in further increases in the Ly α .

Table 11.4

L α emission coefficients in partially ionized regions (all in $\text{erg cm}^3 \text{ s}^{-1}$)

T (K)	Low density $n_e \ll 1.5 \times 10^4 \text{ cm}^{-3}$		High density $n_e \gg 1.5 \times 10^4 \text{ cm}^{-3}$	
	$\frac{4\pi j_{\text{L}\alpha}}{n_e n(\text{H}^0)}$	$\frac{4\pi j_{\text{L}\alpha}}{n_e n_p}$	$\frac{4\pi j_{\text{L}\alpha}}{n_e n(\text{H}^0)}$	$\frac{4\pi j_{\text{L}\alpha}}{n_e n_p}$
10,000	2.56×10^{-24}	2.87×10^{-24}	4.46×10^{-24}	4.25×10^{-24}
12,500	2.62×10^{-23}	2.39×10^{-24}	4.51×10^{-23}	3.53×10^{-24}
15,000	2.23×10^{-22}	2.01×10^{-24}	2.10×10^{-22}	3.06×10^{-24}
20,000	8.89×10^{-22}	1.51×10^{-24}	1.46×10^{-21}	2.34×10^{-24}

- The recombination emission coefficient of Ly α is given by

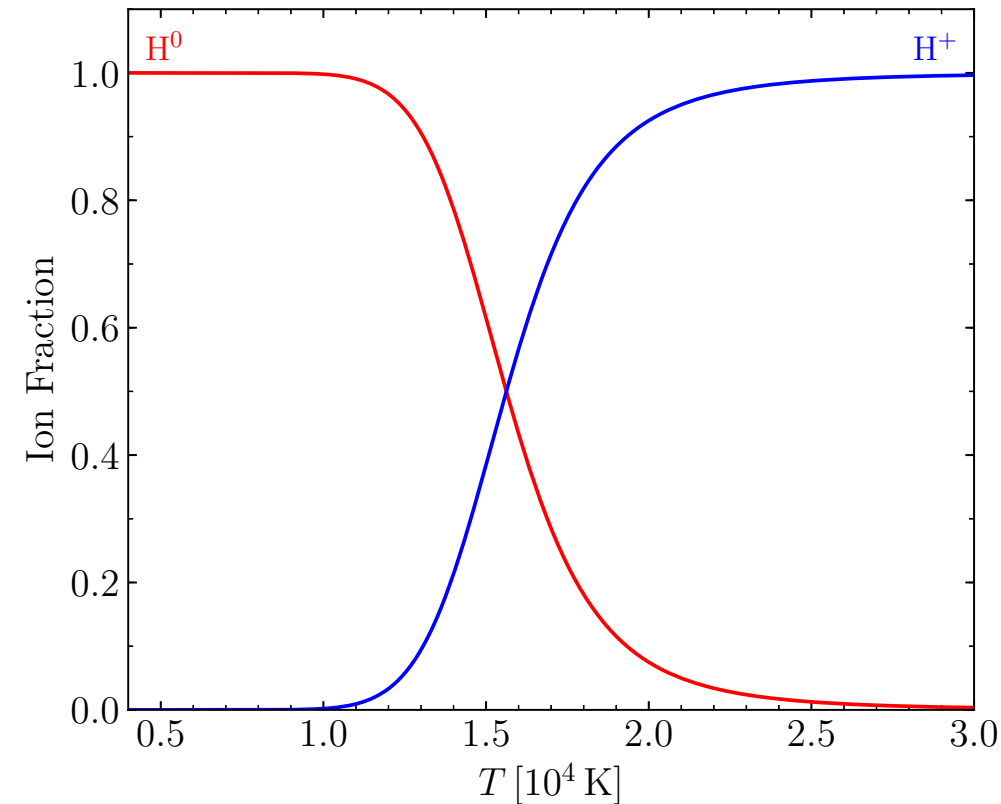
$$\begin{aligned} 4\pi j_{\text{Ly}\alpha} &= n_e n_p \alpha_{2^2P_0}^{\text{eff}} h\nu_{\text{Ly}\alpha} \\ &= n_e n_p (\alpha_B - \alpha_{2^2S}^{\text{eff}}) h\nu_{\text{Ly}\alpha} \end{aligned}$$

Here, numerical values of $\alpha_{2^2S}^{\text{eff}}$ are shown in Table 4.11.

- Collision vs. Recombination

- Note that collisionally excited emission of Ly α increases rapidly with temperature, because of its high threshold (10.2 eV).
- For a half-ionized gas with $n(\text{H}^0) = n_p$:
 - At $T = 10,000$ K, the collisional and recombination contributions to Ly α are roughly the same.
 - At $T = 12,500$ K, the collisional excitations are more important by nearly a factor of ten. However, heating a gas to such a high temperature while maintaining neutrality is nearly impossible.
- For a mostly ionized gas with $n(\text{H}^0) \approx 0.09n_p$:
 - At $T = 12,500$ K, the collisional and recombination contributions to Ly α are approximately equal.

Collisional Ionization Equilibrium



-
- Collisional shift of 2^2S to 2^2P^o at high densities
 - At higher densities, the 2^2S state (resulting from collisional excitation, recombination, or cascading) are collisionally shifted to 2^2P^o and then emit Ly α .
 - The critical density for this process is

$$n_c = \frac{A_{2^2S, 1^2S}}{q_{2^2S, 2^2P^o}^p + q_{2^2S, 2^2P^o}^e} \approx 1.5 \times 10^4 \text{ [cm}^{-3}\text{]} \quad \text{for } n_e \approx n_p.$$

- **Collisional excitation:** Thus, in this high-density limit, the first approximation to the collisional-excitation emission coefficient (including the mixing effect) is

$$4\pi j_{\text{Ly}\alpha}^{\text{coll}} = n_e n(\text{H}^0) (q_{1^2S, 2^2S} + q_{1^2S, 2^2P}) h\nu_{\text{Ly}\alpha}.$$

A better approximation is

$$4\pi j_{\text{Ly}\alpha}^{\text{coll}} = n_e n(\text{H}^0) \sum_{n=2}^3 \sum_{L=0}^{n-1} q_{1^2S, n^2L} h\nu_{\text{Ly}\alpha}$$

- **Recombination:** in high-density limit, the recombination emission coefficients (including the mixing) is

$$4\pi j_{\text{Ly}\alpha}^{\text{rec}} = n_e n_p \alpha_B h\nu_{\text{Ly}\alpha}$$

- Both the collisional and recombination Ly α emission coefficients are larger by factors of ~ 1.5

Table 11.4

$\text{Ly}\alpha$ emission coefficients in partially ionized regions (all in $\text{erg cm}^3 \text{ s}^{-1}$)

T (K)	Low density $n_e \ll 1.5 \times 10^4 \text{ cm}^{-3}$		High density $n_e \gg 1.5 \times 10^4 \text{ cm}^{-3}$	
	Collisional $\frac{4\pi j_{\text{Ly}\alpha}}{n_e n(\text{H}^0)}$	Recombination $\frac{4\pi j_{\text{Ly}\alpha}}{n_e n_p}$	Collisional $\frac{4\pi j_{\text{Ly}\alpha}}{n_e n(\text{H}^0)}$	Recombination $\frac{4\pi j_{\text{Ly}\alpha}}{n_e n_p}$
10,000	2.56×10^{-24}	2.87×10^{-24}	4.46×10^{-24}	4.25×10^{-24}
12,500	2.62×10^{-23}	2.39×10^{-24}	4.51×10^{-23}	3.53×10^{-24}
15,000	2.23×10^{-22}	2.01×10^{-24}	2.10×10^{-22}	3.06×10^{-24}
20,000	8.89×10^{-22}	1.51×10^{-24}	1.46×10^{-21}	2.34×10^{-24}

- Collisional-excitation emission of H α
 - Collisional excitation to any of the levels 3^2S , 3^2P^o , or 3^2D leads to H α emission under Case B conditions.
 - Thus, the first approximation to the collisional-excitation emission coefficient for H α is

$$4\pi j_{H\alpha} = n_e n_p \sum_{L=0}^2 q_{1^2S, 3^2L} h\nu_{H\alpha}.$$

[Table 11.5] H α emission coefficients in partly ionized regions for $n_e = 10^4 \text{ cm}^{-3}$ (in $\text{erg cm}^{-3} \text{ s}^{-1}$)

T (K)	Collisional $\frac{4\pi j_{H\alpha}}{n_e n(H^0)}$	Recombination $\frac{4\pi j_{H\alpha}}{n_e n_p}$
10,000	2.12×10^{-26}	3.54×10^{-25}
12,500	3.47×10^{-25}	2.89×10^{-25}
15,000	2.28×10^{-24}	2.46×10^{-25}
20,000	2.25×10^{-23}	1.81×10^{-25}

- Collisional excitation show a stronger temperature dependence.

If $n(H^0) = n_p$ and $T = 10,000 \text{ K}$, the collisional H α emission is about 8% as large as the recombination emission.

If $n(H^0) = 0.11 n_p$ and $T = 12,500 \text{ K}$, the collisional H α emission is about 19% of the recombination contribution.

- Collisional-excitation of $H\beta$ and higher Balmer lines
 - They are even smaller with respect to the recombination contributions, because of the higher thresholds and smaller cross sections.
 - The degree of ionization of H and the temperature vary strongly as the ionization approaches zero in the transition region of an AGN.
- Therefore, quantitative statements about the total collisionally excited contributions to the various H I line emission depend upon detailed model calculations (as will be discussed in Chapters 13 and 14).
 - In general, (1) the collisionally excited $Ly\alpha$ emission is quite important
 - (2) the collisional excitation adds a small but significant contribution to the $H\alpha$ recombination emission
 - (3) the collisional contributions to $H\beta$ and higher Balmer lines are nearly negligible.
- From these models, for the entire AGN narrow line region (NLR), **the intrinsic Balmer decrement is approximately $H\alpha/H\beta = 3.1$** , which exceeds the recombination value 2.85, resulting from the effects of collisional excitation of $H\alpha$.